Title
THE PERIODIC, ELECTROCHEMICAL CODEPOSITION OF CADMIUM AND TELLURIUM

Authors
Verbrugge, M.W.
Tobias, C.W.

Publication Date
1986-08-01

Lawrence Berkeley Laboratory
UNIVERSITY OF CALIFORNIA

Materials & Molecular Research Division

Submitted to Journal of the Electrochemical Society

THE PERIODIC, ELECTROCHEMICAL CODEPOSITION OF CADMIUM AND TELLURIUM

M.W. Verbrugge and C.W. Tobias

August 1986

Prepared for the U.S. Department of Energy under Contract DE-AC03-76SF00098

DISCLAIMER

LBL-21013

THE PERIODIC, ELECTROCHEMICAL CODEPOSITION OF CADMIUM AND TELLURIUM

Mark W. Verbrugge[†]

and

Charles W. Tobias

Department of Chemical Engineering,
University of California at Berkeley, and
Materials and Molecular Research Division,
Lawrence Berkeley Laboratory,
Berkeley, California 94720

August 1986

Keywords: alloy, electrochemical, electrodeposition

[†] Present address: General Motors Research Laboratories, Warren, Michigan, 48090-9055.

The Periodic, Electrochemical Codeposition of Cadmium and Tellurium

Mark W. Verbrugge and Charles W. Tobias

Abstract

A mathematical model is presented for the codeposition of cadmium and tellurium onto a rotating-disk electrode. The treatment incorporates the equation of convective diffusion for liquid-phase mass transport, Butler-Volmer expressions for charge-transfer reactions, and a thermodynamic model for individual component activities in the solid state. Because of the formation of CdTe, a compound that has a large negative free energy of formation, the cadmium-deposition reaction occurs at potentials substantially positive to its standard electrode potential ($U^{\theta} = -0.40$ V). This reaction, along with the deposition of tellurium ($U^{\theta} = +0.55$ V), produces an electrodeposit that contains cadmium, tellurium, and cadmium telluride. The model can be used to calculate transient current-potential relationships, ionic concentration profiles, and deposit compositions. Transport and kinetic parameters for cadmium and tellurium deposition are reported; a multidimensional optimization routine is used to evaluate physicochemical parameters from experimental data for the codeposition process.

Introduction

The unique properties of CdTe were recognized as early as 1856 (Tibbals, 1909). As reflected by the voluminous literature devoted to this material, CdTe is probably the most extensively studied wide-band-gap, II-VI compound (Aven and Prener, 1967). A number of monographs (*e.g.* Zanio, 1978, and references cited therein) are dedicated exclusively to CdTe . Cadmium telluride materials have found applications in gamma-ray and x-ray spectrometers, electrooptic and acoustooptic modulators, liquid-crystal imaging devices, and as solar-cell materials.

One of the most promising applications of CdTe lies in the fabrication of photovoltaic devices. In 1956, Loferski presented a theoretical treatment to aid in the selection of the optimum semiconductor for photovoltaic solar-energy conversion. The semiconductor yielding the highest maximum efficiency, defined as the ratio of the maximum electrical power output to the solar-power flux incident to the semiconductor surface, was CdTe .

In the present work, we report the determination of transport and kinetic parameters relevant to the electrochemical codeposition of Cd and Te, and we provide a mathematical model representing this codeposition with a periodic cell current. It has been observed by numerous researchers that the phase structure and morphology of alloy deposits[†] can be altered by changing the characteristics of the cell-current waveform (*e.g.*, Puippe and Ibl, 1980). In work related to the present study, we report the influence of a pulse-current source on the Cd-Te-deposit morphology and photovoltaic properties (Verbrugge, 1985). Although pulsing the cell current provides a useful means for improving deposit quality, this mode of operation requires a more sophisticated mathematical analysis, relative to steady-state processes, to predict deposit composition.

[†] Faust (1940) defined alloy deposition as "... any process where two or more metals are codeposited intentionally and in which, due to this codeposition, special properties are imparted to the electroplate." In 1963, Brenner adopted the *Metals Handbook* (Lyman, 1948) definition: "A substance that has metallic properties and is composed of two or more chemical elements of which at least one is a metal." Brenner further modified this with the following: "For practical purposes, we can consider a metallic substance as an alloy if the individual constituents cannot be seen by the unaided eye." Physical chemists usually adopt a more restrictive definition. Seitz (1943) refers to alloys as being either *substitutional* or *interstitial*. In the state of complete order, each phase is said to have developed a *superlattice*. For some chemical systems, the alloy forms only for a fairly definite composition, and a superstructure always exists. Mott and Jones (1958) state that such alloys are more properly called compounds. This is the case for CdTe.

Thin films of CdTe have been prepared by chemical vapor deposition, vacuum evaporation, and electrodeposition processes. As is the case in the present study, most CdTe-electrodeposition processes make use of an aqueous, cadmium sulfate, tellurium dioxide, sulfuric acid electrolyte (Danaher and Lyons, 1978; Panicker *et al.*, 1978; Fulop *et al.*, 1982; Engelken, 1983; Gerritsen, 1984; Takahashi *et al.*, 1984; Uosaki *et al.*, 1984; Lyons *et al.*, 1984; Bhattacharya, 1984). Thin-film electrodeposits have also been formed from nonaqueous solvents (Darkowski and Cocivera, 1985) and from aqueous, potassium cyanide electrolytes (Skyllas-Kazacos, 1983). Since the costs associated with thin-film electrodeposition processes are generally less than those with other thin-film fabrication techniques, the present study should be relevant to the fabrication of large-area, CdTe solar cells.

Because of the low solubility of TeO_2 in aqueous solutions – the maximum concentration of $HTeO_2^+$ is $\approx$ 0.001 M (Issa and Awad, 1954) – the Cd^{2+} ion concentration may also be chosen to be sufficiently low ($\approx$ 0.1 M) so that dilute-solution transport theory (Newman, 1973) can be applied. There is a large free energy associated with the formation of CdTe, and hence the composition-dependent thermodynamic properties of the solid state must be taken into account in modeling the electrodeposition process. To account for deviations from ideal behavior, a thermodynamic model is incorporated into the alloy-deposition analysis to describe the activity of the individual components in the electrodeposit. Engelken and Van Doren (1985) have incorporated the same thermodynamic model for the solid state in their analyses for the steady-state electrodeposition of II-IV and III-V compounds. White *et al.* (1977) have modeled a codeposition system incorporating a homogeneous, electrochemical reaction. Pesco and Cheh (1985) have treated steady-state, alloy-electrodeposition processes for systems with a nonuniform current distribution. Beauchamp (1985) has developed a one-dimensional model for the pulsed electrodeposition of alloys. Menon and Landau (1985) have modeled cells with nonuniform current distribution and included unsteady-state effects. Except for the work of Engelken and Van Doren, these models do not take into account nonideal behavior in the solid state. The models are useful, however, for the treatment of chemical systems that form a deposit wherein the activity of each constituent is equal to its mole fraction. White *et al.* studied the electrodeposition of

Cu with very small amounts of Fe codeposited. Pesco and Cheh, Beauchamp, and Menon and Landau compared their model results to experimental data obtained from the codeposition of Pb and Sn.

The schematic diagram of the electrodeposit-electrolyte interface in Fig. 1 can help clarify the salient features of our model work. For a dilute liquid phase, ion-ion interactions are negligible, and the dilute-solution equation of convective diffusion can be applied to evaluate $c_i(t, y)$, the concentration of reactant or product species in the neutral liquid phase. For solutions of high ionic strength and dilute in reacting ions, the diffuse portion of the double layer will not change significantly in structure, and the potential drop across this region of charge separation can be neglected for highly conductive, well supported solutions. The inner edge of the diffuse portion of the double layer is the outer Helmholtz plane (OHP), which represents the plane of closest approach for the *non-specifically* adsorbed ions. Immediately adjacent to the electrode surface is the inner Helmholtz plane (IHP), where solution species can be *specifically* adsorbed to the electrodeposit surface. Since specific adsorption is dependent on electrodeposit-solution interactions, and since it is not included in our model, the rate constants measured for Cd and Te electrodeposition may have to be altered in an attempt to match experimental and calculated results, as the CdTe surface may specifically adsorb species differently from the Cd or Te surfaces. In general, the IHP poses a very difficult region to quantify. In this study, the last region of interest, the forming electrodeposit, is assumed to contain three species in equilibrium: Cd, Te, and CdTe (Panicker *et al.*, 1978). Due to the low bulk concentration of $HTeO_2^+$, the deposit growth rate is slow and does not significantly influence the fluid dynamics.

The most accessible experimental variables are the total cell current and the potential of the working electrode with respect to a suitable reference. For this reason, we shall compare calculated polarization curves with those obtained by experiment. It is also possible to compare the predicted and measured electrodeposit composition, but this is a more difficult task and would probably provide less insight. Too little electrodeposit is formed to allow accurate determination of the composition by deposit dissolution and subsequent quantitative analysis. (Only thin-film deposits were formed because thick deposits tend to acquire a roughened surface and affect the fluid flow, thus impairing the chances

for successful comparison of experiment with theory.) There are a number of other *ex situ* analysis techniques, although they do not appear as quantitative or convenient as theoretical-experimental comparisons of polarization curves obtained in alloy electrodeposition processes. Swathirajan (1985) presents support for the use of *in situ* acquisition of cell current-potential characteristics, and subsequent comparison with theoretical calculations, in order to investigate electrochemical stripping experiments of alloy electrodeposits, in lieu of *ex situ* surface analysis techniques.

Physicochemical Parameters for Cd and Te Electrodeposition

In the following sections, we discuss the electrodeposition of Te and Cd. The measured physicochemical parameters for Te electrodeposition and Cd electrodeposition are then used to mathematically model the codeposition of Te and Cd onto a rotating-disk electrode (RDE). The reactions relevant to the study are listed in Table 1. In all these deposition studies, 0.3-M-H_2SO_4 was used as supporting electrolyte. The Cd^{2+} species was obtained by adding cadmium sulfate, and the $HTeO_2^+$ species resulted from adding tellurium dioxide to the electrolyte (reaction *vi* of Table 1). Both glassy-carbon and polycrystalline, cadmium disk electrodes were used. Standard metallographic polishing techniques were used to remove all projections greater than one micron in height. The electrodes were cleaned with a dilute nitric acid solution before each experiment. The potential of the working electrode was measured against a mercury-mercurous sulfate reference electrode. A Princeton Applied Research model 173 potentiostat/galvanostat controlled the operation of the cell; an Interstate F77 function generator was used with the potentiostat/galvanostat. The data were stored on a Nicolet 1090A digital oscilloscope and later transferred to an HP9825A computer.

The aqueous, sulfuric acid electrolytes were prepared from analytical-reagent-grade chemicals and distilled water that was passed through a Culligan water purification unit consisting of an organic trap, a deionizer, and a microfilter. The specific conductance of the treated water was 15 Mohm-cm. Nitrogen, first equilibrated with a similar electrolyte, was bubbled through the cell solution for 1 hour

Table 1. Reactions

Interfacial Reactions:

Reaction Designation	Standard Electrode Potential (V)	Electrochemical Reaction
i †	0.64	$Hg_2SO_4 + 2e^- = 2Hg + SO_4^{2-}$
ii	0.55	$HTeO_2^+ + 3H^+ + 4e^- = Te + 2H_2O$
iii	0.00	$H^+ + e^- = \frac{1}{2}H_2$
iv	-0.40	$Cd^{2+} + 2e^- = Cd$
v	-0.92	$Te + 2e^- = Te^{2-}$

Homogeneous Reactions:

Reaction Designation	Homogeneous Reaction
vi	$TeO_2 + H^+ = HTeO_2^+$
vii	$Cd + Te = CdTe$

† Reaction *i* represents the reference-electrode reaction used in the experimental portion of this work.

prior to experiments. A nitrogen atmosphere was maintained above the electrolyte during the experiments.

The primary factor limiting the rate of CdTe electrodeposition is the mass-transfer resistance of the discharging $HTeO_2^+$ ion. This is due to low solubility of TeO_2 in aqueous, sulfuric acid solutions. Since there is very little $HTeO_2^+$ in solution, relative to the concentration of Cd^{2+}, the $HTeO_2^+$ species quickly becomes diffusion limited if a one-to-one mole ratio (1:1) of Cd to Te is desired in the electrodeposit. If a direct-current source is used to form the CdTe electrodeposit,

approximately 1:1 CdTe can be produced if the cell-current density is $\frac{3}{2} \times i_{lim,HTeO_2^+}$, where $i_{lim,HTeO_2^+}$ is the steady-state, diffusion-limited current density of the $HTeO_2^+$ species,

$$i_{lim,HTeO_2^+} = -\frac{D_{HTeO_2^+} c^b_{HTeO_2^+}}{4F\,\delta_{HTeO_2^+}}. \qquad [1]$$

The Nernst diffusion-layer thickness (Levich, 1962) for the $HTeO_2^+$ species is

$$\delta_{HTeO_2^+} = 1.612\left(\frac{D_{HTeO_2^+}}{\nu}\right)^{\frac{1}{3}}\left(\frac{\nu}{\omega}\right)^{\frac{1}{2}}. \qquad [2]$$

The factor of $\frac{3}{2}$ preceding $i_{lim,HTeO_2^+}$ is required since four moles of electrons are reacted per mole of Te deposited by reaction *ii*, and two moles of electrons are reacted per mole of Cd deposited by reaction *iv*. (Note that Faraday's law can be used to state $i_l = n_l F N_{i,l}/s_{i,l}$. For 1:1 CdTe, $N_{HTeO_2^+} = N_{Cd^{2+}}$.)

The tellurium solution chemistry is complex, and Eq. *ii* of Table 1 is only an approximation for the $HTeO_2^+$/Te electrode processes. Electroanalytical studies of tellurium in the +4 state are presented in the fundamental work of Lingane and Niedrach (1948 and 1949). The chemistry of TeO_2 in sulfuric acid solutions is addressed in the work of Flowers *et al.* (1959). The solubility of TeO_2, which limits the rate of CdTe electrodeposition in aqueous, sulfuric acid solutions, was investigated by Schuhmann (1925), who postulated the species in solution to be $HTeO_2^+$ and electrode reaction *ii* of Table 1. Issa and Awad (1954) studied the solubility of TeO_2 in aqueous HCl and buffered solutions. Cheng (1961) noted that the sulfate electrolytes yielded a slightly higher solubility than a number of other inorganic salts he studied. Dutton and Cooper (1966) have reviewed analytical work on the oxides and oxyacids of tellurium, and later Cooper (1971) published a treatise on the element Te and its unique chemistry.

In the present work, the diffusion coefficient of the $HTeO_2^+$ species, $D_{HTeO_2^+}$, was calculated

from limiting-current experiments. The 0.001-M-$HTeO_2^+$/0.3-M-H_2SO_4, aqueous electrolyte was maintained at 20 °C; the calculated diffusion coefficient is 9.4×10^{-6} cm^2/s. The resulting Levich plot is shown in Fig. 2 for the 20 °C experiment, as well as for similar experiments conducted at 55, 70, and 85 °C.

Knowledge of the temperature dependence of $D_{HTeO_2^+}$ is of value since CdTe is often electrodeposited at higher temperatures to obtain large grain deposits with superior electronic properties. At these higher temperatures, the solubility of TeO_2 is still low relative to $CdSO_4$ (the soluble salt used to place Cd^{2+} in solution), and a direct-current-density source equal to $\frac{3}{2} \times i_{lim,HTeO_2^+}$ can still be used to deposit approximately 1:1 CdTe. In order to obtain 1:1 CdTe and use the $\frac{3}{2} \times i_{lim,HTeO_2^+}$ estimate for the cell-current density, $D_{HTeO_2^+}(T)$ must be known for all temperatures, as can be seen from Eq. [1]. The approximate relationship

$$\frac{D_i \mu}{T} \approx constant \qquad [3]$$

is frequently employed (Bird *et al.*, 1960), where μ is the solution viscosity. For the aqueous H_2SO_4-$HTeO_2^+$ solutions analyzed in this work, the average value of the constant in Eq. [3] was 3.04×10^{-10} $cm-g/s^2-K$ with a standard deviation, weighted over the four temperatures, of 0.014×10^{-10} $cm-g/s^2-K$. Table 2 lists the temperature dependence of the solution transport properties. Handbook values were used for the electrolyte viscosity.

Table 2. Transport properties of Te-deposition electrolyte.

Temperature (K)	Viscosity $\left(\frac{g}{cm - s}\right)$	Diffusion Coefficient $\left(\frac{cm^2}{s}\right)$	$\frac{D_{HTeO_2^+}\mu}{T}$ $\left(\frac{cm - g}{K - s}\right)$
293	0.010	9.4×10^{-6}	3.21×10^{-10}
328	0.0050	2.0×10^{-5}	3.05×10^{-10}
343	0.0041	2.4×10^{-5}	2.87×10^{-10}
358	0.0034	3.2×10^{-5}	3.04×10^{-10}

Triangular current-sweep chronopotentiometric experiments were conducted on this system to obtain the kinetic parameters of reaction *ii* in Table 1. The technique developed by the authors was used to construct the theoretical response to the triangular current sweep (Verbrugge and Tobias, 1985a). A symmetry factor of 0.1 and an exchange-current density of 2.0 mA/cm^2, based on bulk ionic concentrations and unit activity of the electrodeposit, were found to best represent the experimental data.

The electrode potential at which the Cd-deposition reaction occurs, reaction *iv* of Table 1, can be used to approximate the potential at which 1:1 CdTe can be deposited from an aqueous, sulfuric acid electrolyte. Because of the low solubility of TeO_2, the mass transfer of the $HTeO_2^+$ species usually limits the rate of Te deposition. No matter how much more cathodic the electrode potential is driven, the rate of Te deposition remains nearly constant ($c^{surf}_{HTeO_2^+} \approx 0$), and the added cathodic potential is used only to increase the rate of Cd deposition. For this reason, knowledge of the electrode-kinetic behavior of reaction *iv* is an important aspect in the understanding of CdTe-electrodeposition processes.

Limiting-current experiments, analogous to those described in the Te-deposition section, were conducted to obtain $D_{Cd^{2+}}$. The 0.10-M-$CdSO_4$/0.3-M-H_2SO_4 electrolyte was maintained at 23 °C; the calculated value for $D_{Cd^{2+}}$ is 3.7×10^{-6} cm^2/s. Since the CdTe -electrodeposition process is less affected by the Cd^{2+} transport, relative to the $HTeO_2^+$ transport, the temperature dependence of $D_{Cd^{2+}}$ will not be discussed. We (1985a) report for the diffusion coefficient of the Cd^{2+} species in a 0.0058-M-$CdSO_4$/0.25-M-K_2SO_4 electrolyte $D_{Cd^{2+}} = 3.6 \times 10^{-6}$ cm^2/s . Since $D_{Cd^{2+}}$ is nearly identical in the two solutions, we have a strong indication that there are no significant ion-ion interactions, only ion-solvent interactions, and that dilute-solution transport equations can be used to analyze these experimental systems. Furthermore, in the aqueous, sulfuric acid electrolyte, $D_{HTeO_2^+} = 9.6 \times 10^{-6}$ cm^2/s , which is significantly greater than $D_{Cd^{2+}}$. The $HTeO_2^+$ complex is rather large, with only one positive charge spread throughout the ion. Consequently, it is probably less solvated and can diffuse faster through solution than the smaller Cd^{2+} species (the concentration gradient of both species being equal), which probably has a larger hydration shell.

In general, the Cd-deposition current-potential curve is difficult to duplicate theoretically with a Butler-Volmer electrode-kinetic expression. We (1985a) have investigated the electrodeposition of Cd from an aqueous, potassium sulfate electrolyte. A symmetry factor of 0.15 and an exchange-current density of 9.1 mA/cm^2, based on the bulk concentration of Cd^{2+} and unit deposit activity, were found to best represent the current-potential relationship for the discharge of Cd^{2+} from the sulfuric acid electrolyte.

Mathematical Analysis for the Periodic Codeposition of Cd and Te

The liquid phase. The one-dimensional equation of convective diffusion is used to describe the mass transport of species i :

$$\frac{\partial c_i}{\partial t} + v_y \frac{\partial c_i}{\partial y} = D_i \frac{\partial^2 c_i}{\partial y^2} \quad . \qquad [4]$$

Close to the disk surface, the normal velocity is (Schlichting, 1979)

$$v_y \cong -0.51023\ \omega^{3/2}\ \nu^{-1/2}\ y^2 \quad . \qquad [5]$$

The initial condition and boundary conditions are

$$c_i(0,y) = c_i^b \quad , \qquad [6]$$

$$c_i(t,\infty) = c_i^b \quad , \qquad [7]$$

and

$$\frac{\partial c_i(t,0)}{\partial y} = \frac{1}{FD_i} \sum_l \frac{s_{i,l}\ i_l(t)}{n_l} \quad , \qquad [8]$$

where the summation indicates that a species can be involved in more than one electrochemical reaction.

The electrode-reaction l can be expressed as

$$n_l\, e^- \underset{k_{a,l}}{\overset{k_{c,l}}{\rightleftarrows}} \sum_i s_{i,l}\, M_i^{z_i} \quad . \qquad [9]$$

Equation [9] is a general expression for an electrochemical reaction, from which any of the electrochemical reactions listed in Table 1 can be represented.

Equation [4] provides a good representation of the ionic mass transport for systems with large Schmidt numbers, small disk radii, low exchange-current densities, highly-conductive electrolytes, and low concentrations of reacting species (Newman, 1966). For the electrodeposition process, subscript i refers to $HTeO_2^+$, H^+, Cd^{2+}, and Te^{2-}, the four ionic species participating in the electrochemical reactions of Table 1. Four convective diffusion equations are written for the four species; the solution

to this system of equations yields the surface concentrations of the reactant and product species and the partial current densities of reactions *ii*, *iii*, *iv*, and *v*. It should be noted that the hydrogen evolution reaction may have a non-uniform distribution due to the high concentration of H^+. However, the hydrogen evolution reaction is very slow on the electrodeposited material, and the high kinetic resistance tends to promote a uniform reaction distribution. Usually the codeposition process takes place with high current efficiency, and little hydrogen evolution occurs.

The liquid-electrodeposit interface. A Butler-Volmer electrode-kinetic equation is used to relate the partial current density of the electrochemical reaction l, the surface concentrations of the species participating in the reaction, and the electrode potential. The four electrode-kinetic equations represent reactions *ii*, *iii*, *iv*, and *v* of Table 1, respectively:

$$\frac{i_{ii}}{4F} = k_{a,ii}\, e^{(1-\beta_{ii})4fV}\, a_{Te} - k_{c,ii}\, e^{-\beta_{ii}4fV} (c_{HTeO_2^+})(c_{H^+})^3 \qquad [10]$$

$$\frac{i_{iii}}{F} = k_{a,iii}\, e^{(1-\beta_{iii})fV} (p_{H_2})^{1/2} - k_{c,iii}\, e^{-\beta_{iii}fV}\, c_{H^+} \qquad [11]$$

$$\frac{i_{iv}}{2F} = k_{a,iv}\, e^{(1-\beta_{iv})2fV}\, a_{Cd} - k_{c,iv}\, e^{-\beta_{iv}2fV}\, c_{Cd^{2+}} \qquad [12]$$

$$\frac{i_{v}}{2F} = k_{a,v}\, e^{(1-\beta_{v})2fV}\, c_{Te^{-2}} - k_{c,v}\, e^{-\beta_{v}2fV}\, a_{Te} \qquad [13]$$

In addition, the sum of the partial current densities must equal the cell-current density,

$$\sum_{l=ii}^{v} i_l = i_{cell} \quad . \qquad [14]$$

The potential V in Eqs. [10]-[13] represents the potential difference between the working electrode and a standard hydrogen electrode, corrected for ohmic drop. V is given by

$$V = E + \left[U^{\theta}_{ref} - \frac{1}{n_{ref}\, f} \sum_i s_{i,ref} \ln c_{i,ref} \right] - i_{cell}\, r \quad , \qquad [15]$$

where E is the measured cell potential.

The partial current densities in Eqs. [10]-[13] couple the convective diffusion equations through the boundary condition given by Eq. [8]. The activity of Cd, a_{Cd}, and Te, a_{Te}, is treated in the following section.

The Electrodeposit. To evaluate the component activities in the electrodeposit, we shall make use of Jordan's (1970) regular associated solution (RAS) theory. Jordan developed this theory in order to describe mathematically the liquidus curves for the Cd-Te and Zn-Te systems. Since the same three species are present in the solid phase (Cd, Te, and CdTe), we use the same model.

The RAS theory adapted for the Cd-Te-CdTe system contains the assumption that departures from ideal-solution behavior are due to short-range, nearest-neighbor interactions, which are taken into account by identifying the activity coefficients γ_{Cd}, γ_{Te}, and γ_{CdTe}, with those of a regular, ternary solution, making use of *interchange energies* for Cd-Te, Cd-CdTe , and Te-CdTe interactions. These expressions can be combined with the Gibbs energy of formation for CdTe (reaction *vii*, Table 1),

$$\Delta G_{\mathrm{CdTe}} = -RT \ln \frac{a_{\mathrm{CdTe}}}{a_{\mathrm{Cd}}\, a_{\mathrm{Te}}} \quad . \qquad [16]$$

If the interchange energies for Cd-CdTe and Te-CdTe interactions are taken equal, the activities can be approximated as

$$a_{\mathrm{Te}} = \frac{\bar{x}_{\mathrm{Te}} - \bar{x}_{\mathrm{Cd}} + P}{1 + P} \exp\left[\frac{\alpha(\bar{x}_{\mathrm{Cd}})^2}{RT} \right] , \qquad [17]$$

$$a_{\mathrm{Cd}} = \frac{\bar{x}_{\mathrm{Cd}} - \bar{x}_{\mathrm{Te}} + P}{1 + P} \exp\left[\frac{\alpha(\bar{x}_{\mathrm{Te}})^2}{RT} \right] , \qquad [18]$$

and

$$a_{\mathrm{CdTe}} = \frac{1-P}{1+P} \exp\left[\frac{\alpha}{2RT} (1 - 4\overline{x}_{\mathrm{Te}}\,\overline{x}_{\mathrm{Cd}}) \right] , \qquad [19]$$

where

$$P = \left[1 - \overline{x}_{\mathrm{Te}}\,\overline{x}_{\mathrm{Cd}} (1 - \beta_{act}^2) \right]^{\frac{1}{2}} . \qquad [20]$$

β_{act} is the degree of dissociation at $\overline{x}_{\mathrm{Cd}} = \overline{x}_{\mathrm{Te}} = 0.5$; the overbar has been used to denote atomic mole fractions. Equations [17]-[20] represent a one-parameter model for the electrodeposit thermodynamics, since the Gibbs free energy of formation for CdTe can be used to eliminate α or β_{act}.

The atomic mole fractions for Te, $\overline{x}_{\mathrm{Te}}$, and Cd, $\overline{x}_{\mathrm{Cd}}$, can be obtained by integrating the appropriate partial current densities:

$$\overline{x}_{\mathrm{Cd}} = \frac{\int_{t_{RSAT}}^{t} 2i_{iv}\, dt}{\int_{t_{RSAT}}^{t} (i_{ii} + 2i_{iv} - 2i_{v})\, dt} , \qquad [21]$$

and

$$\overline{x}_{\mathrm{Te}} = 1 - \overline{x}_{\mathrm{Cd}} . \qquad [22]$$

In these expressions, the time interval from t_{RSAT} to t is required to deposit one relevant surface-activity thickness ($RSAT$). The $RSAT$ is the depth of deposit that is used to evaluate a surface composition. This allows us to introduce a length scale into the solid-state thermodynamic model. A more complete discussion of the $RSAT$ is provided elsewhere (Verbrugge and Tobias, 1985b).

The *liquid-electrodeposit interface* section and the *electrodeposit* section provide boundary-condition information for the mass-transport problem. In these two sections there are ten unknowns: i_{ii}, i_{iii}, i_{iv}, i_{v}, V, E, a_{Cd}, a_{Te}, x_{Cd}, and x_{Te}. These are balanced by the following ten, independent equations: [10], [11], [12], [13], [14], [15], [17], [18], [21], and [22]. The system of equations is solved by the method of superposition; the numerical method used for these types of problems is presented elsewhere (Verbrugge and Tobias, 1985b). In applying the superposition technique, we used Nisancioglu

and Newman's (1974) flux-step solution. A Newton-Raphson routine was employed to iteratively solve the resulting system of equations. This model was combined with an optimization routine (Verbrugge and Tobias, 1985a) to fit the physicochemical parameters to the data. In the next section of this treatment, we analyze the periodic electrodeposition process with model and experimental results.

Results of the Proposed Model

The current source used in the theoretical calculations and experimental work is shown in Fig. 3. The maximum pulse-current density is $1.23 \times i_{lim,HTeO_2^+}$. As previously discussed, $\frac{3}{2} \times i_{lim,HTeO_2^+}$ yields nearly 1:1 CdTe. For the 30 $\frac{A}{m^2}$ (3 $\frac{mA}{cm^2}$) maximum cathodic current source used in this study, we would expect the Te atomic mole fraction to be greater than 0.5. The input parameters to the computer program are listed in Table 3. In the following discussion, we analyze the base-case behavior and explain how the input kinetic constants and β_{act} were chosen. In Fig. 4, a plot of the ionic surface concentrations is shown. A surface-concentration plot is not shown for Te^{2-} since the current due to reaction v of Table 1 was insignificant under these conditions, although the rate constants for this reaction were set to high values. Te^{2-} did not form for two reasons. First, Te is attracted to Cd and CdTe in the deposit, thus Te has a suppressed deposit activity and the cathodic term in Eq. [13] is strongly reduced. Secondly, the electrode potential required to deposit CdTe is significantly more anodic than the -0.92 volts standard electrode potential of reaction v. It should be noted that reaction v cannot be dropped from the analysis *a priori*. It is commonly observed in the electrodeposition of pure Te (unit activity in the deposit) that Te^{2-} is formed prior to hydrogen evolution (Lingane and Niedrach, 1948; Jamieson and Perone, 1969; Shinagawa *et al.*, 1977; Barbier *et al.*, 1978). In addition, more cathodic potentials result if larger cathodic currents are used; larger cathodic currents could be used to create a deposit with higher Cd content. As can be seen in Table 3, the bulk concentration of $HTeO_2^+$ is much lower than that of Cd^{2+}. The $HTeO_2^+$ concentration reaches a minimum near the end of the first on-time, when $\frac{c^{surf}_{HTeO_2^+}}{c^{b}_{HTeO_2^+}} = 0.16$ and $t = 0.5$ s.

Table 3. Input Parameters. †

Quantity					Units
c_i^b	1.0×10^{-6}	3.0×10^{-4}	1.0×10^{-4}	0.0	$\frac{\text{mol}}{\text{cm}^3}$
D_i	9.4×10^{-6}	9.3×10^{-5}	3.6×10^{-6}	9.3×10^{-5}	$\frac{\text{cm}^2}{\text{s}}$
$k_{a,l}$	3.4×10^{-42}	5.0×10^{-12}	7.8×10^{5}	∞	‡
$k_{c,l}$	6.7×10^{-5}	5.0×10^{-12}	1.8×10^{-8}	∞	‡
n_l	4	1	2	2	---
r	0				$\Omega - \text{cm}^2$
$RSAT$	1.0×10^{-7}				cm
α	-1.7×10^{5}				$\frac{\text{J}}{\text{mol}}$
β_{act}	6.4×10^{-5}				---
β_l	0.26	0.50	0.20		---
δ_i	0.0058	0.0034	0.0011	0.0034	cm
ρ_o	0.0010				$\frac{\text{kg}}{\text{cm}^3}$
$\hat{\rho}_i$	0.049 (Te)	0.077 (Cd)	0.0025 (CdTe)		$\frac{\text{mol}}{\text{cm}^3}$

† Optimized results were used for $k_{a,l}$, $k_{c,l}$, α, β_{act} , and β_l . For species entries, denoted by subscript i on the variable quantity, $HTeO_2^+$ is at the far left, followed by H^+, Cd^{2+}, and Te^{2-}, respectively, unless otherwise stated. For reaction entries, denoted by subscript l on the variable quantity, reaction ii is at the far left, followed by iii , iv , and v , respectively.

‡ The rate-constant units are reaction dependent. For anodic rate constants, the units are: mol /[cm^2 - s - $\prod_i$(anodic reactant concentration units)$^{s_{i,l}}$]. For cathodic rate constants, the exponent $s_{i,l}$ is replaced by $-s_{i,l}$.

During the following off-time, diffusion and convection resupply the electrode surface with $HTeO_2^+$

ions from the bulk electrolyte, and the concentration of $HTeO_2^+$ increases until the beginning of the next on-time. This process is repeated over the subsequent cycles. The Cd^{2+} and H^+ species incur little mass-transport resistance, and their surface concentrations do not differ significantly from their bulk concentrations under these conditions.

The partial current densities for reaction *ii*, *iii*, and *iv* are given in Fig. 5. At the beginning of the on-time (0 seconds for the first cycle), reaction *ii* supplies most of the current, and the $HTeO_2^+$ surface concentration is reduced. As the $HTeO_2^+$ ion becomes mass-transfer limited, reaction *iv* increases in rate and more Cd deposits. During the off-time, Cd dissolves and Te continues to electrodeposit. For these conditions, there is very little hydrogen evolution. Both experimental and theoretical results indicate that the electrodeposition process takes about 5 cycles to reach a uniform and sustained periodic state. About 1.5 *RSAT* are deposited per cycle. It is the electrodeposit's influence that prolongs the approach to steady state; the surface-concentration profiles reach a periodic state prior to the fifth cycle, as seen in Fig. 4. The partial current densities during a particular cycle are dependent on the *RSAT* concentration formed during the previous cycle. It is because of this dependence on the previous cycle that the system oscillates about the uniform periodic state until the fifth cycle.

In Fig. 6 the electrodeposit mole fractions are presented for the base conditions. The mole fractions are related to the atomic mole fractions by the following equations:

$$x_{Te} = \frac{\bar{x}_{Te} - \bar{x}_{Cd} + P}{1 + P}, \qquad [23]$$

$$x_{Cd} = \frac{\bar{x}_{Cd} - \bar{x}_{Te} + P}{1 + P}, \qquad [24]$$

and

$$x_{CdTe} = \frac{1 - P}{1 + P}. \qquad [25]$$

As expected, due to the Gibbs free energy of formation of CdTe being large and negative, very little

free Cd exists for $\bar{x}_{Cd} < 0.5$; most of the Cd is present in the CdTe . It can also be seen that during the off-times Cd dissolves, and free Te is released into the electrodeposit, which increases the Te mole fraction x_{Te} .

The experimental and calculated electrode-potential behavior is presented in Figs. 7 and 8 for the fifth cycle, after the system has reached a periodic state. To construct the theoretical curve in Fig. 7 (labeled INITIAL), the measured rate parameters ($k_{a,l}$, $k_{c,l}$, and, β_{act}) for Te deposition and Cd deposition were used. In an attempt to force reaction v to take place with the current source specified in Fig. 3, $D_{Te^{2-}}$ was set to a high value, as were the rate constants for reaction v ; the ratio of the rate constants is fixed by the standard electrode potential. To better represent the experimental curve, a multidimensional optimization routine was used to minimize the difference between the calculated and experimental potential response, the results of which are presented in Fig. 8. The optimization routine was not sensitive to the kinetic parameters for H_2 evolution or Te dissolution to produce Te^{2-}. β_{act} was set equal to 0.055 to construct the INITIAL curve in Fig. 7, as this was the value Jordan used in his high temperature experiments. The optimization routine changed this parameter more than any other. The final values of the optimized parameters are listed in Table 3. The shape of the INITIAL curve in Fig. 7 resembles the experimental curve. After the optimization routine operates on the model, the resultant FINAL curve in Fig. 8 is displaced closer to the experimental curve. It should be noted that the ordinate is different in Figs. 7 and 8. The proposed fit solution in Fig. 8 does not represent an entirely satisfactory result, although the theoretical solution does remain in a potential region near the experimental curve. To elucidate the behavior of the model, a sensitivity analysis of the optimized parameters is addressed in the following sections.

The effect of changing the Te-deposition rate constants is depicted in Fig. 9. If the rate constants $k_{a,ii}$ and $k_{c,ii}$ are set larger by an order of magnitude, or if a larger symmetry factor is used, more Te is incorporated into the electrodeposit. The periodic state is reached sooner since Cd dissolution from the lower Cd-content deposit is suppressed during the off-time. A uniform and sustained

periodic state is reached by the third cycle.

If the Cd kinetic constants are reduced by an order of magnitude, the system reaches a steady state after about 2 cycles, as seen in Fig. 10. Because the system is more sensitive to the Cd-electrodeposition kinetics, a steady state is reached more quickly in Fig. 10 than in Fig. 9. The system is less sensitive to Te-electrodeposition kinetics, reaction *ii*, because the major obstacle to Te deposition is the $HTeO_2^+$-mass-transfer resistance.

If the hydrogen rate constants are increased by four orders of magnitude, the partial current densities during the deposition process are represented by Fig. 11. For this case, H_2 is evolved during the on-time, slightly reducing the Te and Cd deposition rates, relative to the base-case deposition rates. During the off-time, dissolved H_2 present at low concentration is oxidized to H^+, and at the end of the off-time both Cd and Te electrodeposit, in contrast to any of the previous cases.

If β_{act} is increased by an order of magnitude, increasing the dissociation of CdTe, the electrodeposit composition history in Fig. 12 results. Comparing Fig. 12 to the base-case deposit-mole-fraction plot in Fig. 6, we can see that a higher concentration of free Te results with the increased CdTe dissociation.

The mole-fraction plot in Fig. 13 shows that the CdTe content in the electrodeposit can be increased by specifying an on-time to off-time ratio of 3:1 for the cell-current source, instead of the 1:1 ratio used in the base conditions. Since the $HTeO_2^+$ species is mass-transfer limited during the majority of the on-time, the Cd^{2+} rate of reaction increases throughout the on-time (*e.g.* Fig. 5). During the extra on-time in the 3:1 mode of operation, more Cd deposits, which combines with Te in the electrodeposit to form CdTe. More cathodic potentials result in the 3:1 mode of operation, and some hydrogen evolution occurs during the last part of the on-time. The CdTe content in the electrodeposit can also be increased by increasing the maximum cell current during the on-time. The partial current densities for a maximum cathodic current density equal to twice that of the base conditions are shown in Fig. 14. In this mode of operation, the $HTeO_2^+$ species quickly becomes mass-transfer limited, and the rate of Cd deposition increases during the on-time. With the added amount of Cd in the

electrodeposit, a larger Cd corrosion current is observed during the off-time. It can also be seen that H_2 begins to evolve during the on-time. The system reaches a uniform and sustained periodic state after the second cycle since about 3 $RSAT$ are deposited during the on-time, and the system is nearly driven to a steady state by the end of each on-time.

Conclusions

Due to the increasing demand for thin-film alloys with precisely controlled composition and structure, researchers are beginning to address the quantitative modeling of codeposition processes. In this study, we have coupled a thermodynamic description of the electrodeposit with transient convective diffusion equations for the electrolyte species; Butler-Volmer equations, written for each charge-transfer reaction, relate the equations describing the electrolyte and solid phases. The model shows reasonable agreement with results obtained from the periodic co-electrodeposition of Cd and Te onto a rotating-disk electrode. A more sophisticated model would incorporate double-layer adsorption, the capacitance of the double layer (for processes in which the pulsed-current frequency is comparable to, or larger than, the inverse of the characteristic time for the double-layer charging processes), and a more general treatment of the electrodeposit, including solid-state kinetic processes.

Acknowledgment

This work was supported by the Director, Office of Energy Research, Office of Basic Energy Sciences, Materials Sciences Division of the Office of the U.S. Department of Energy, under contract no. DE-AC03-76SF00098.

Nomenclature

a_i	surface activity of component i
c_i	concentration of species i, $\frac{\text{mol}}{\text{cm}^3}$
c_i^b	bulk concentration of species i, $\frac{\text{mol}}{\text{cm}^3}$
$c_{i,ref}$	reference-electrode compartment concentration of species i, $\frac{\text{mol}}{\text{cm}^3}$
D_i	diffusion coefficient of species i, $\frac{\text{cm}^2}{\text{s}}$
e^-	symbol for an electron
E	electrode potential relative to the reference electrode, V
f	F/RT, V^{-1}
F	Faraday's constant, 96487 $\frac{\text{C}}{\text{equivalent}}$
i	cell-current density, $\frac{\text{mA}}{\text{cm}^2}$
i_l	partial current density for reaction l, $\frac{\text{mA}}{\text{cm}^2}$
$k_{a,l}$	anodic rate constant of reaction l
$k_{c,i}$	cathodic rate constant of reaction l
M_i	symbol for chemical formula of species i
n_l	number of electrons in reaction l
$N_{i,l}$	flux of species i corresponding to reaction l, $\text{mol/cm}^2\text{-s}$
p_{H_2}	hydrogen partial pressure, atm
r	cell ohmic resistance, $\Omega - \text{cm}^2$

R	universal gas constant, 8.314 $\frac{\text{J}}{\text{mol} - \text{K}}$
$RSAT$	relevant surface-activity thickness, cm
$s_{i,l}$	stoichiometric coefficient of species i in reaction l
t	time, s
T	absolute temperature, K
$U_l{}^{\theta}$	standard electrode potential for reaction l, V
v_y	normal velocity component to a rotating-disk electrode, $\frac{\text{cm}}{\text{s}}$
x_i	molecular mole fraction of species i
$\overline{x}_i$	atomic mole fraction of species i
y	normal distance from the electrode surface, cm
α	interchange energy, $\frac{\text{J}}{\text{mol}}$
β_{act}	degree of CdTe dissociation at $\overline{x}_{\text{Te}} = \overline{x}_{\text{Cd}} = 0.5$
β_l	symmetry factor for reaction l
δ_i	Levich diffusion layer thickness of species i, cm
ν	kinematic viscosity, $\frac{\text{cm}^2}{\text{s}}$
ρ_o	solvent mass density, $\frac{\text{kg}}{\text{cm}^3}$
$\hat{\rho}_i$	species i molar density, $\frac{\text{mol}}{\text{cm}^3}$
ω	disk rotation speed, $\frac{\text{radian}}{\text{s}}$

Literature Cited

Aven, M. and Prener, J. S., editors, *Physics and Chemistry of II-VI Compounds*, Wiley, New York, 1967.

Barbier, M. J. *et al.*, "Electrochemical Study of Tellurium Oxido-reduction in Aqueous Solutions," *J. Electroanal. Chem.*, **94**, 1978, 47.

Beauchamp, C. R., "A Mathematical Model for the Pulsed Electrodeposition of Alloys," Las Vegas, Nevada Meeting of the Electrochemical Society, October, 1985, Abstract 216.

Bhattacharya, R. N. and Rajeshwar, K., "Electroless Deposition of CdTe Thin Films," *J. Electrochem. Soc.*, **131**, 1984, 939.

Bird, R. B. *et al.*, *Transport Phenomena*, Wiley, New York, 1960.

Brenner, A., *Electrodeposition of Alloys, Principles and Practice*, volume 1, Academic Press, New York, 1963.

Cheng, K. L., "Analysis of Lead Telluride with an Accuracy to Better than 0.1%," *Anal. Chem.*, **33**, 1961, 761.

Cooper, W. C., *Tellurium*, Van Nostrand Reinhold, New York, 1971.

Danaher, W. J. and Lyons, L. E., "Photoelectrochemical Cell with Cadmium Telluride Film," *Nature*, **271**, 1978, 139.

Darkowski, A. and Cocivera, M., "Electrodeposition of Cadmium Telluride using Phosphine Telluride," *J. Electrochem. Soc.*, **132**, 1985, 2768.

Dutton, W. A. and Cooper, W. C., "The Oxides and Oxyacids of Tellurium," *Chem. Revs.*, **66**, 1966, 657.

Engelken, R. D., "An Analysis of the Electrodeposition Process for Cadmium Telluride Thin Film," Ph.D. Thesis, University of Missouri-Rolla, MI, 1983.

Engelken, R. D. and Van Doren, T. P., "Ionic Electrodeposition of II-VI and III-V Compounds," *J. Electrochem. Soc.*, **132**, 1985, 2904 and 2910.

Faust, C. L., "Electrodeposition of Alloys, 1930 to 1940," *Trans. Electrochem. Soc.*, **78**, 1940, 383.

Flowers, R. H. *et al.*, "Basic Properties of the Dioxides of Group VI-I," *J. Inorg. Nucl. Chem.*, **9**, 1959, 155.

Fulop, G. *et al.*, "High-efficiency Electrodeposited Cadmium Telluride Solar Cells," *Appl. Phys. Lett.*, **40**, 1982, 327.

Gerritsen, H. J., "Electrochemical Deposition of Photosensitive CdTe and ZnTe on Tellurium," *J. Electrochem. Soc.*, **131**, 1984, 136.

Issa, I. M. and Awad, S. A., "The Amphoteric Properties of Tellurium Dioxide," *J. Phys. Chem.*, **58**, 1954, 948.

Jamieson, R. A. and Perone, S. P., "Polarographic, Coulometric, and Stationary Electrode Studies of the Electroreduction of Te(IV) in Alkaline Solution," *J. Electroanal. Chem.*, **23**, 1969, 441.

Jordan, A. S., "A Theory of Regular Associated Solutions applied to the Liquidus Curves of the Zn-Te and Cd-Te Systems," *Metal. Trans.*, **1**, 1970, 239.

Lingane, J. J. and Niedrach, L. W., "Potentiometric Titration of +4 and +6 Selenium and Tellurium with Chromous Ion," *J. Am. Chem. Soc.*, **70**, 1948, 1997.

Lingane, J. J. and Niedrach, L. W., "Polarography of Selenium and Tellurium. II. The +4 States,"

ibid., **71**, 1949, 196.

Loferski, J. J., "Theoretical Considerations Governing the Choice of the Optimum Semiconductor for Photovoltaic Solar Energy Conversion," *J. Appl. Phys.*, **27**, 1956, 777.

Lyman, T., editor, *Metals Handbook*, rev. ed., Am. Soc. for Metals, Cleveland, Ohio, 1948.

Lyons, L. E. *et al.*, "Cathodically Electrodeposited Films of Cadmium Telluride," *J. Electroanal. Chem.*, **168**, 1984, 101.

Menon, M. and Landau, U., "Thickness and Composition Variations along Electrodes in Alloy Plating - A Numerical Model," and "Current Distribution Modeling in Cells with Forced Convection Including Unsteady-state Effects," Las Vegas, Nevada Meeting of the Electrochemical Society, October, 1985, Abstracts 217 and 224.

Mott, N. F. and Jones, H., *The Theory of the Properties of Metals and Alloys*, Dover Publications, Inc., New York, 1958.

Newman, J., "Current Distribution on a Rotating Disk below the Limiting Current," *J. Electrochem. Soc.*, **113**, 1966, 1235.

Newman, J., *Electrochemical Systems*, Prentice-Hall, Englewood Cliffs, New Jersey, 1973.

Nisancioglu, K. and Newman, J., "Transient Convective Diffusion to a Disk Electrode," *J. Electroanal. Chem.*, **50**, 1974, 23.

Panicker, M. P. R. *et al.*, "Cathodic Deposition of CdTe from Aqueous Electrolytes," *J. Electrochem. Soc.*, **125**, 1978, 566.

Pesco, A. M. and Cheh, H. Y., "Current Distribution during the Deposition of Tin-Lead Alloys," Las Vegas, Nevada Meeting of the Electrochemical Society, October, 1985, Abstract 218.

Puippe, J. Cl. and Ibl, N., "The Morphology of Pulse-Plated Deposits," *Plating*, **67**, 1980, 68.

Schlichting, H., *Boundary-Layer Theory*, Seventh Edition, McGraw-Hill Book Company, New York, 1979.

Schuhmann, R., "The Free Energy and Heat Content of Tellurium Dioxide and of Amorphous and Metallic Tellurium. The Reduction Potential of Tellurium," *J. Am. Chem. Soc.*, **47**, 1925, 356.

Seitz, F., *The Physics of Metals*, McGraw-Hill Book Company, Inc., New York and London, 1943.

Shinagawa, M. *et al.*, "Studies on the Prewave of Tellurium and Its Photo-effect," *J. Electroanal. Chem.*, **75**, 1977, 809.

Skyllas-Kazacos, M., "Electrodeposition of CdSe and CdSe+CdTe Thin Films from Cyanide Solutions," *ibid.*, **148**, 1983, 233.

Swathirajan, S., "Potentiodynamic and Galvanostatic Stripping Methods for Characterization of Alloy Electrodeposition Process and Product," *J. Electrochem. Soc.*, **133**, 1986, 671.

Takahashi, M. *et al.*, "Composition and Electronic Properties of Electrochemically Deposited CdTe Films," *J. Appl. Phys.*, **55**, 1984, 3879.

Tibbals, C. A., "A Study in Tellurides," *J. Am. Chem. Soc.*, **31**, 1909, 902.

Uosaki, K. *et al.*, "The Photoelectrochemical Behavior of Electrochemically Deposited CdTe Films," *Electrochim. Acta*, **29**, 1984, 279.

Verbrugge, M. W., "The Periodic Electrodeposition of Alloys," Ph.D. Thesis, University of California at Berkeley, CA, 1985.

Verbrugge, M. W. and Tobias, C. W., "Triangular Current-Sweep Chronopotentiometry at Rotating Disk and Stationary, Planar Electrodes," *J. Electroanal. Chem.*, **196**, 1985a, 243.

Verbrugge, M. W. and Tobias, C. W., "A Mathematical Model for the Periodic Electrodeposition of Multicomponent Alloys," *J. Electrochem. Soc.*, **132**, 1985b, 1298.

White, R., "Potential-Selective Deposition of Copper from Chloride Solutions Containing Iron," *ibid.*, **124**, 1977, 669.

Zanio, K., *Cadmium Telluride*, Semiconductors and Semimetals, volume 13, Academic Press, New York, 1978.

Figure Captions

Figure 1. Schematic illustration of the electrodeposit, interface, and liquid phase. IHP refers to inner Helmholtz plane, and OHP refers to outer Helmholtz plane.

Figure 2. Levich plots for $HTeO_2^+$ at various temperatures. The system temperature in °C is listed as a parameter. The diffusion coefficients are listed in Table 2.

Figure 3. Base-case cell-current density.

Figure 4. Base-case, dimensionless ionic surface concentrations.

Figure 5. Base-case, partial current densities. Under these conditions, reaction v does not take place.

Figure 6. Base-case, integrated deposit mole fractions.

Figure 7. Electrode potential for the deposition process. No adjustable parameters were used to construct the theoretical curve labeled INITIAL.

Figure 8. Electrode potential for the deposition process. The ordinate is different from Fig. 7. An optimization routine was used to fit $k_{c,i}$, β_i, β_{act}.

Figure 9. Parametric analysis: tellurium-deposition rate constants $k_{a,ii}$, and $k_{c,ii}$ are increased by an order of magnitude relative to the base conditions.

Figure 10. Parametric analysis: cadmium-deposition rate constants $k_{a,iv}$ and $k_{c,iv}$ decreased by an order of magnitude relative to the base conditions.

Figure 11. Parametric analysis: hydrogen-evolution rate constants $k_{a,iii}$ and $k_{c,iii}$ increased by an order of magnitude relative to the base conditions.

Figure 12. Parametric analysis: solid-state dissociation factor β_{act} increased by an order of magnitude relative to the base conditions.

Figure 13. Parametric analysis: on-time to off-time ratio for the cell-current density set to 3:1.

Figure 14. Parametric analysis: maximum, cathodic pulse-current density twice that of the base condition.

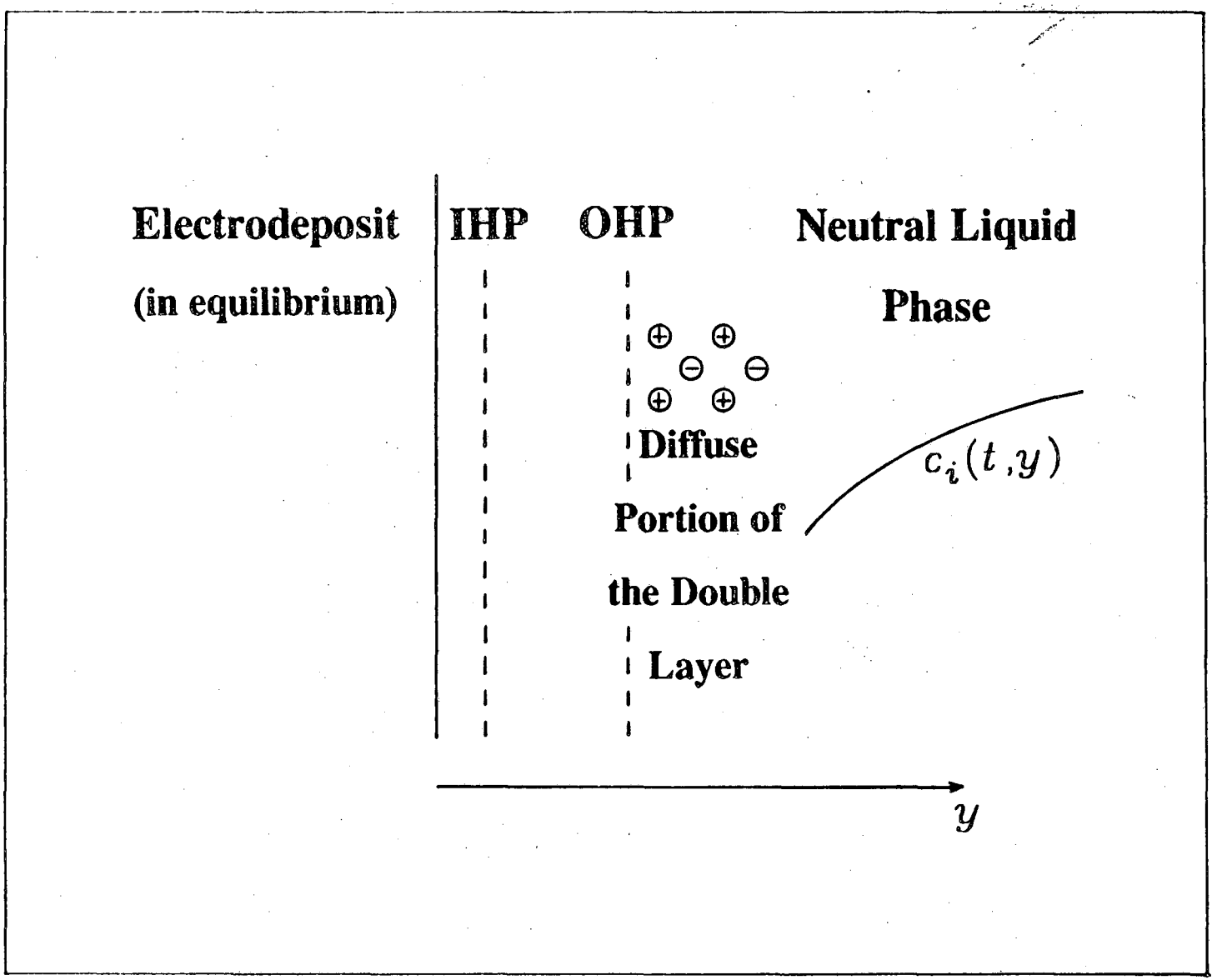
Electrodeposit
(in equilibrium)
IHP
OHP
Neutral Liquid
Phase
Diffuse
Portion of
the Double
Layer
$c_i(t,y)$
y

FIGURE 1.

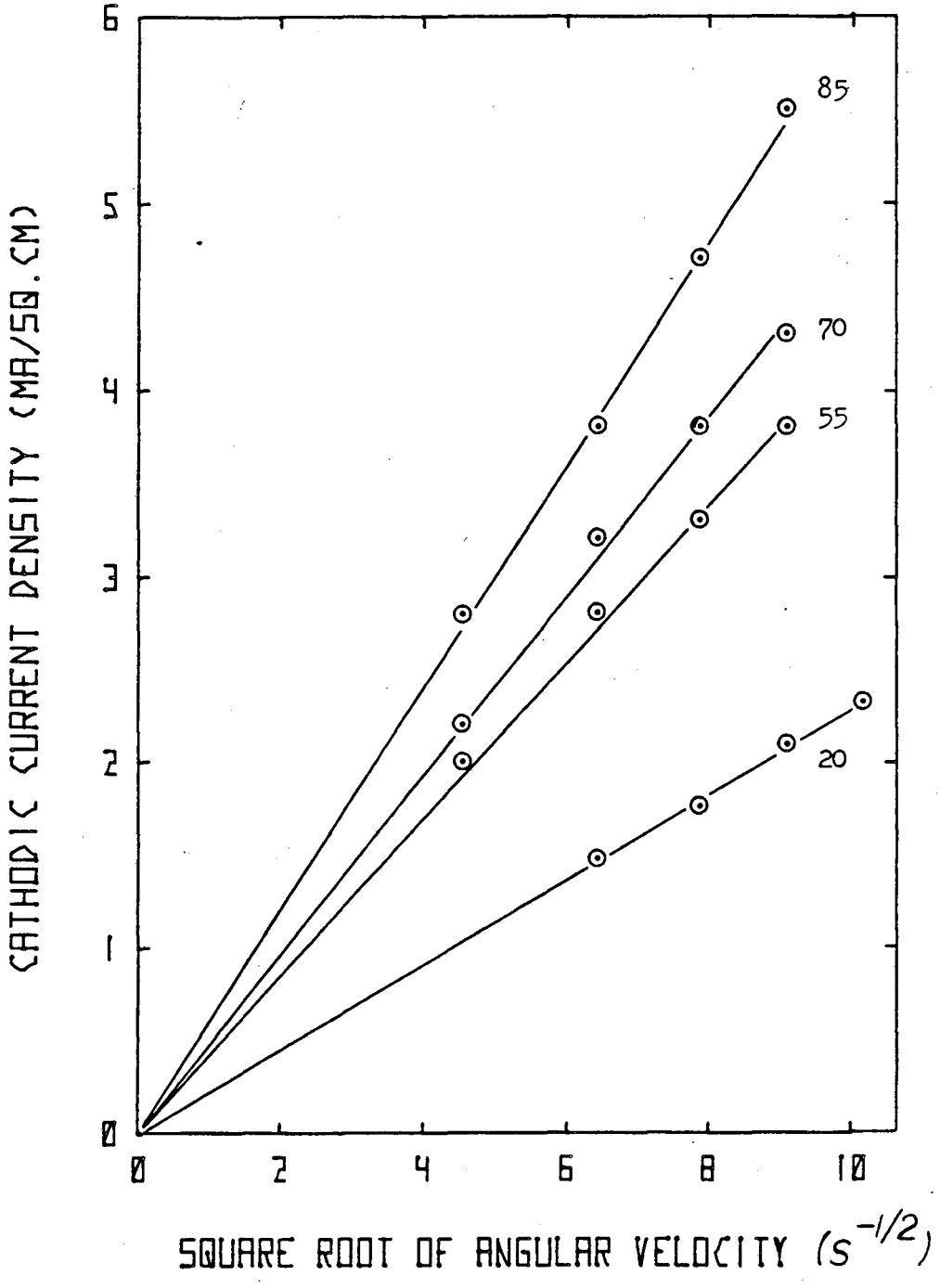
CATHODIC CURRENT DENSITY (MA/SQ.CM)
0
1
2
3
4
5
6
0
2
4
6
8
10
85
70
55
20
SQUARE ROOT OF ANGULAR VELOCITY ($s^{-1/2}$)

FIGURE 2.

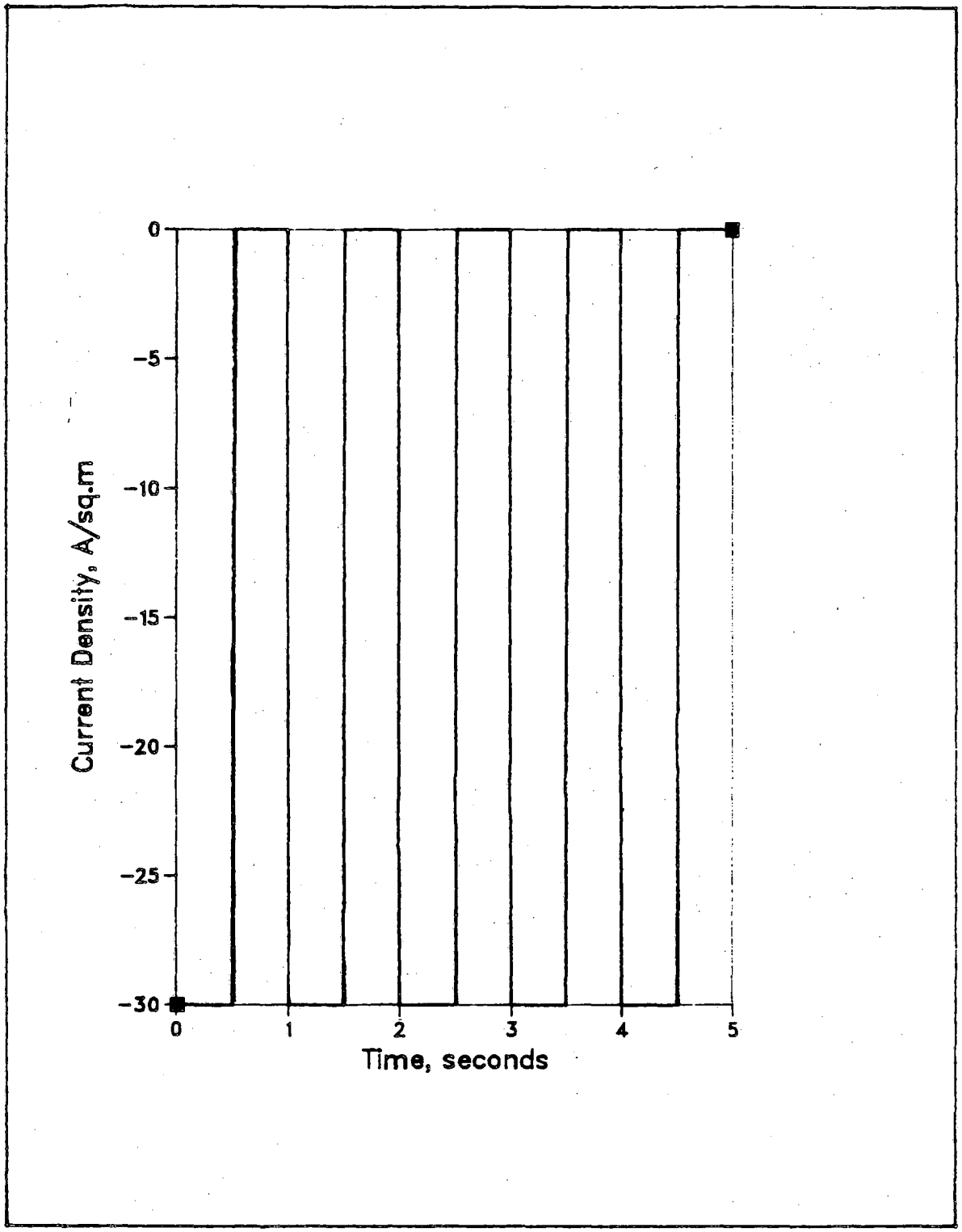

FIGURE 3.

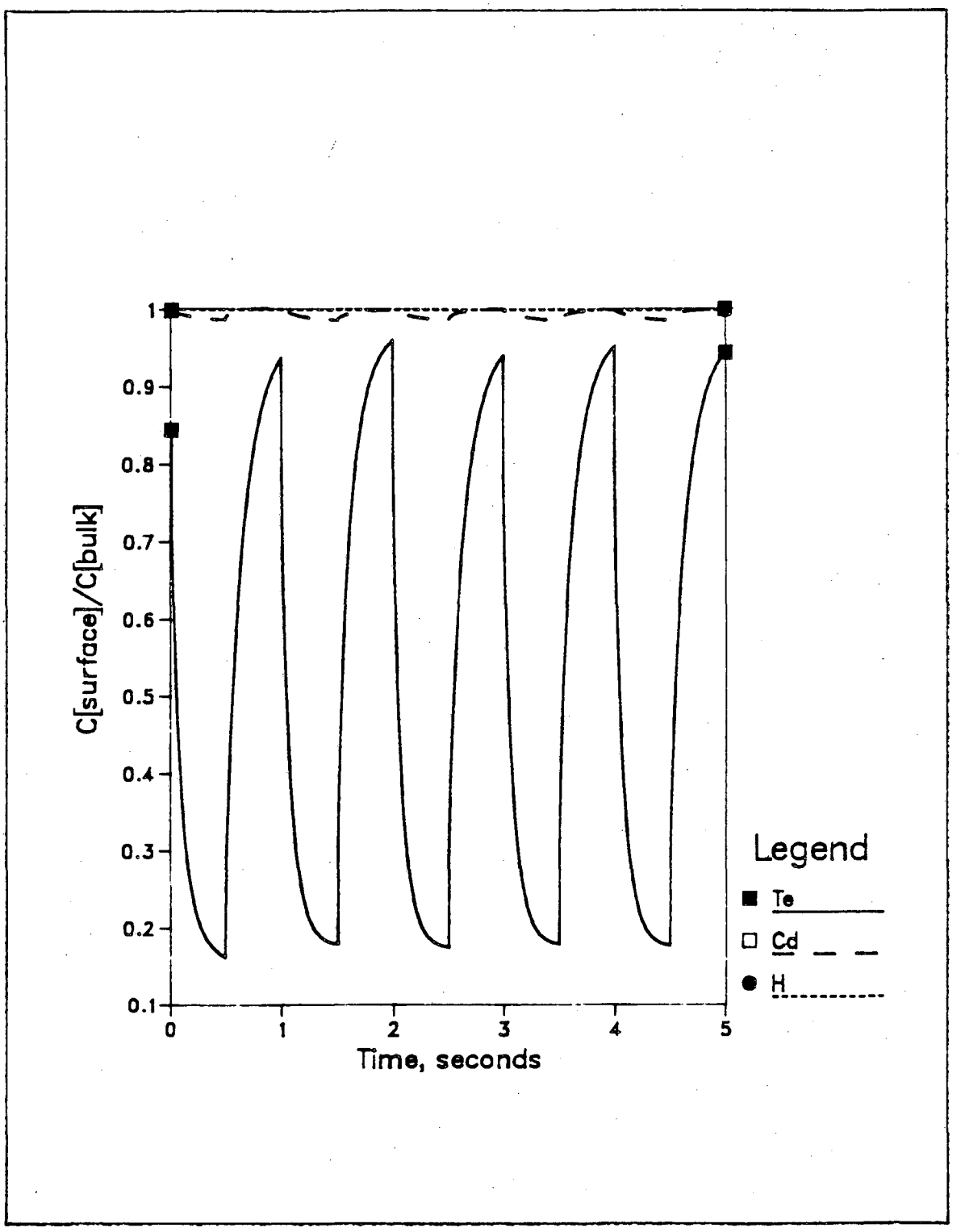
C[surface]/C[bulk]
1
0.9
0.8
0.7
0.6
0.5
0.4
0.3
0.2
0.1
0
1
2
3
4
5
Time, seconds
Legend
Te
Cd
H

FIGURE 4.

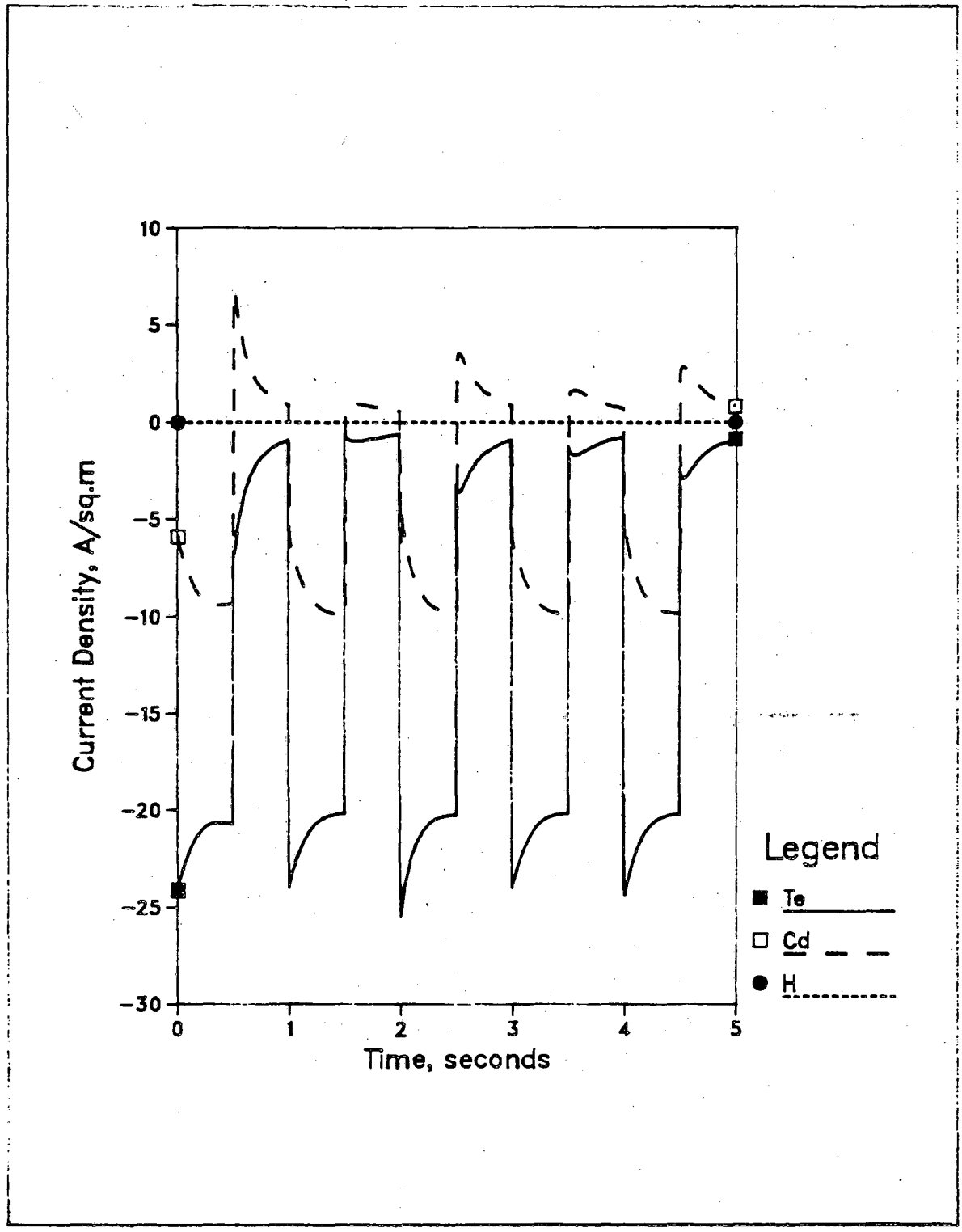
10
5
0
-5
-10
-15
-20
-25
-30
Current Density, A/sq.m
0
1
2
3
4
5
Time, seconds
Legend
Te
Cd
H

FIGURE 5.

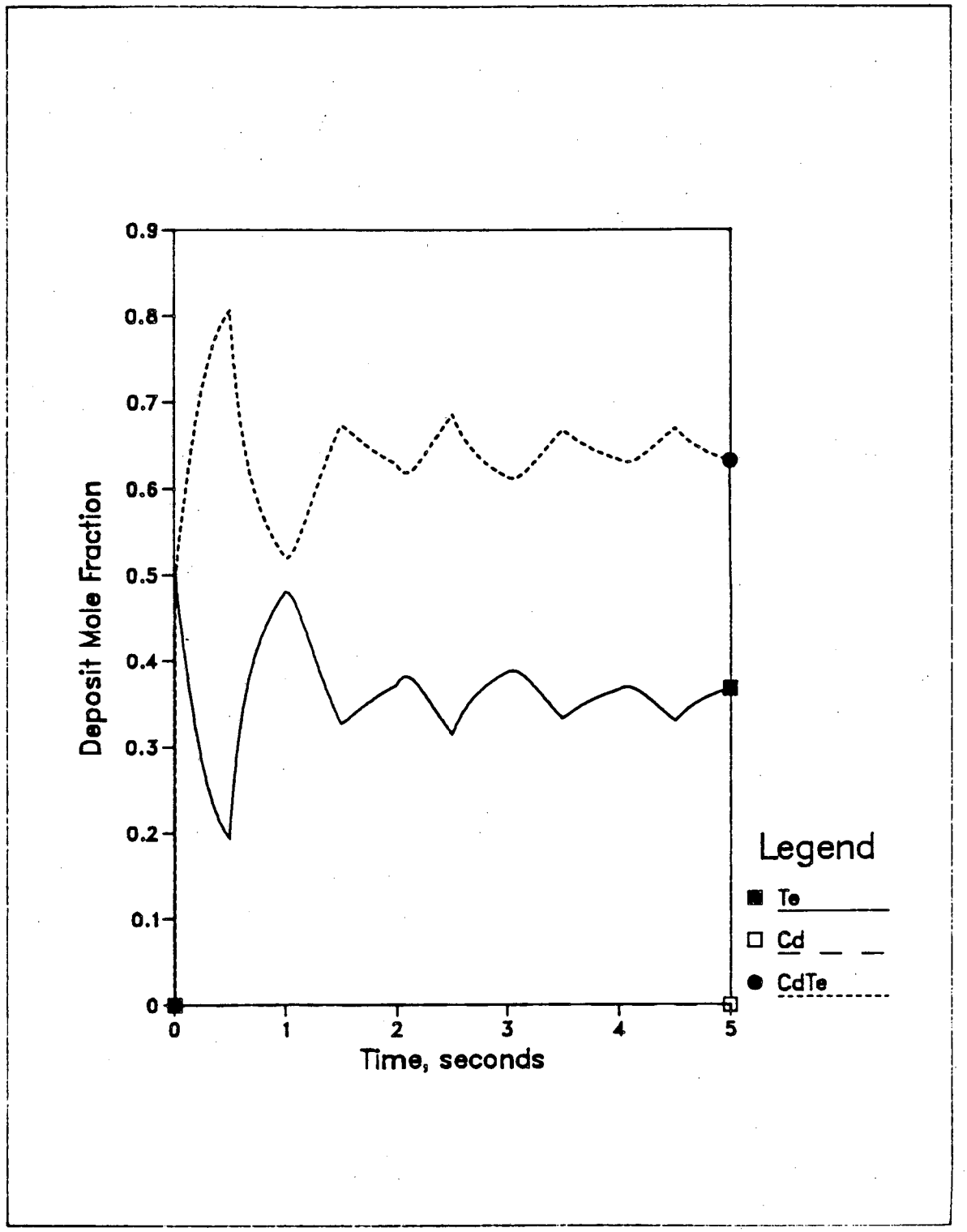
0.9
0.8
0.7
0.6
0.5
0.4
0.3
0.2
0.1
0
Deposit Mole Fraction
0
1
2
3
4
5
Time, seconds
Legend
Te
Cd
CdTe

FIGURE 6.

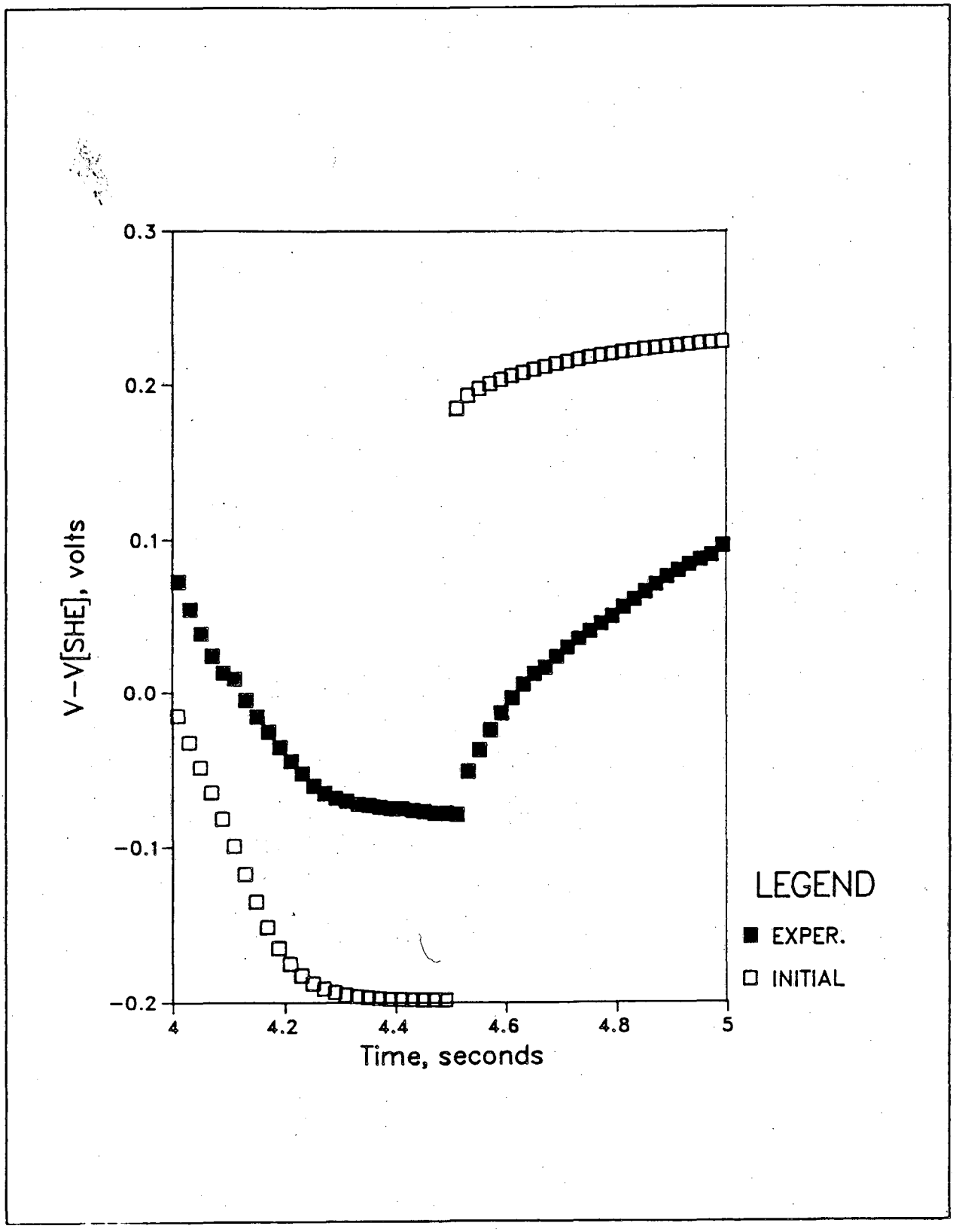
0.3
0.2
0.1
0.0
−0.1
−0.2
V−V[SHE], volts
4
4.2
4.4
4.6
4.8
5
Time, seconds
LEGEND
EXPER.
INITIAL

FIGURE 7.

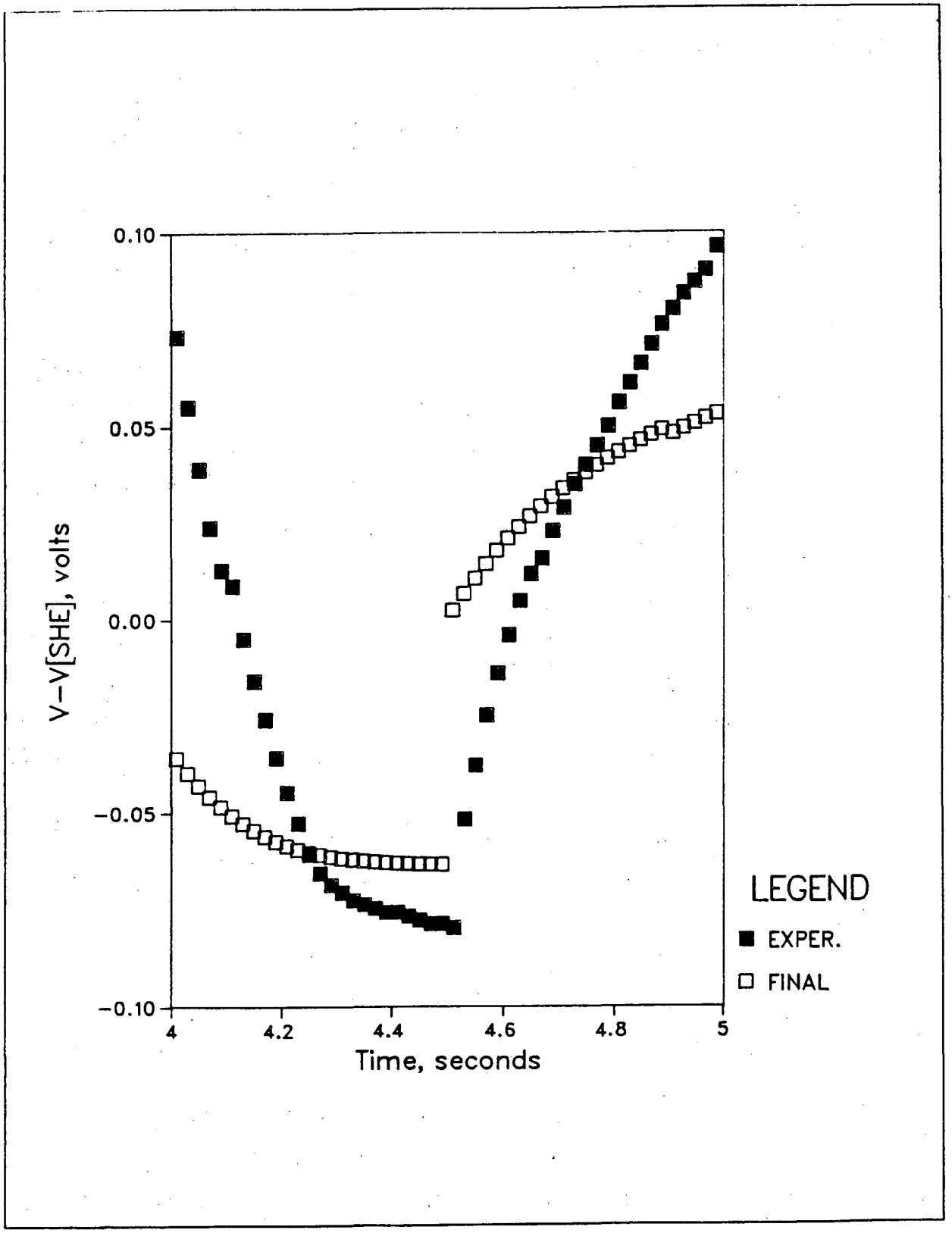
0.10
0.05
0.00
−0.05
−0.10
V−V[SHE], volts
4
4.2
4.4
4.6
4.8
5
Time, seconds
LEGEND
EXPER.
FINAL

FIGURE 8.

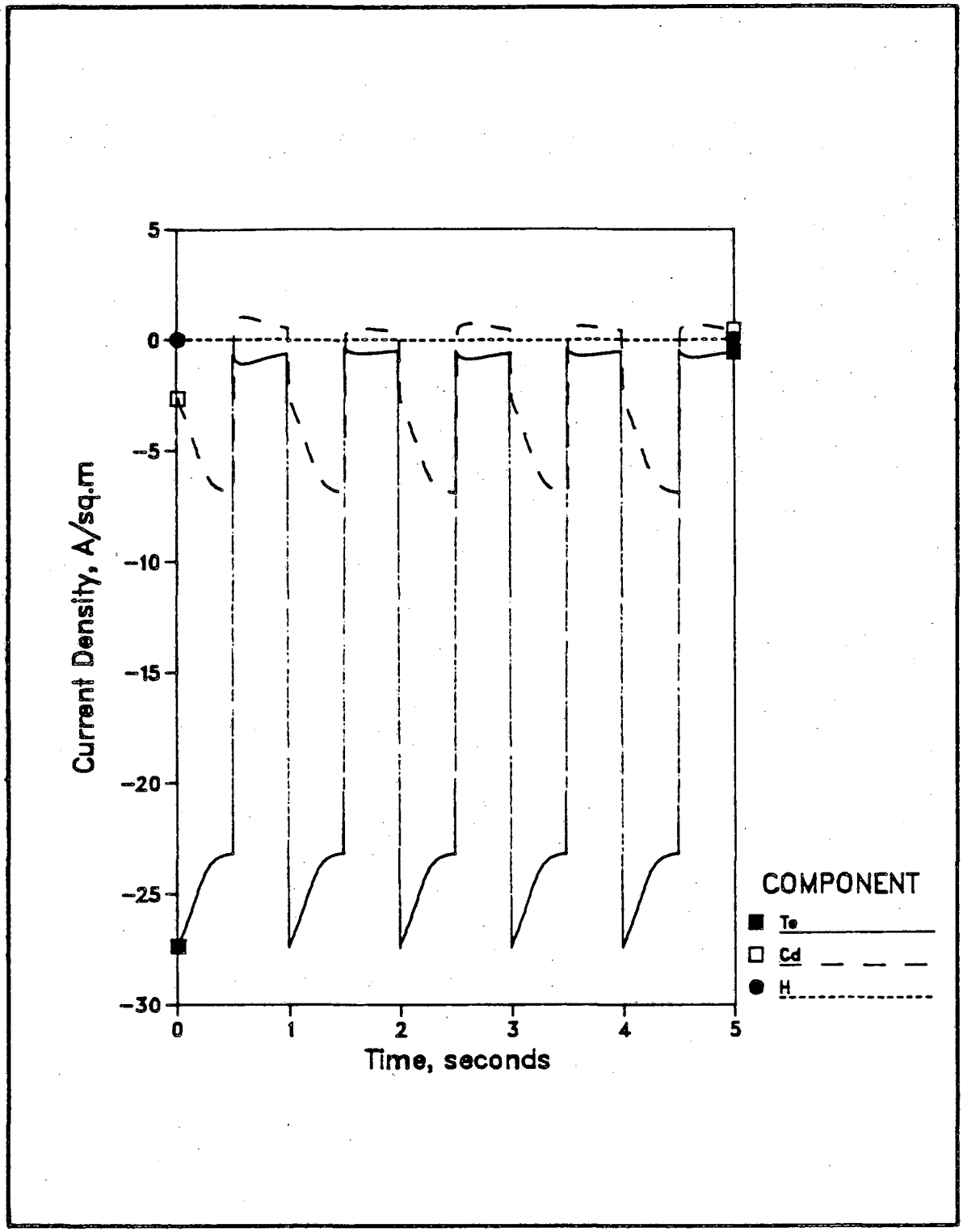
5
0
-5
-10
-15
-20
-25
-30
Current Density, A/sq.m
0
1
2
3
4
5
Time, seconds
COMPONENT
Te
Cd
H

FIGURE 9.

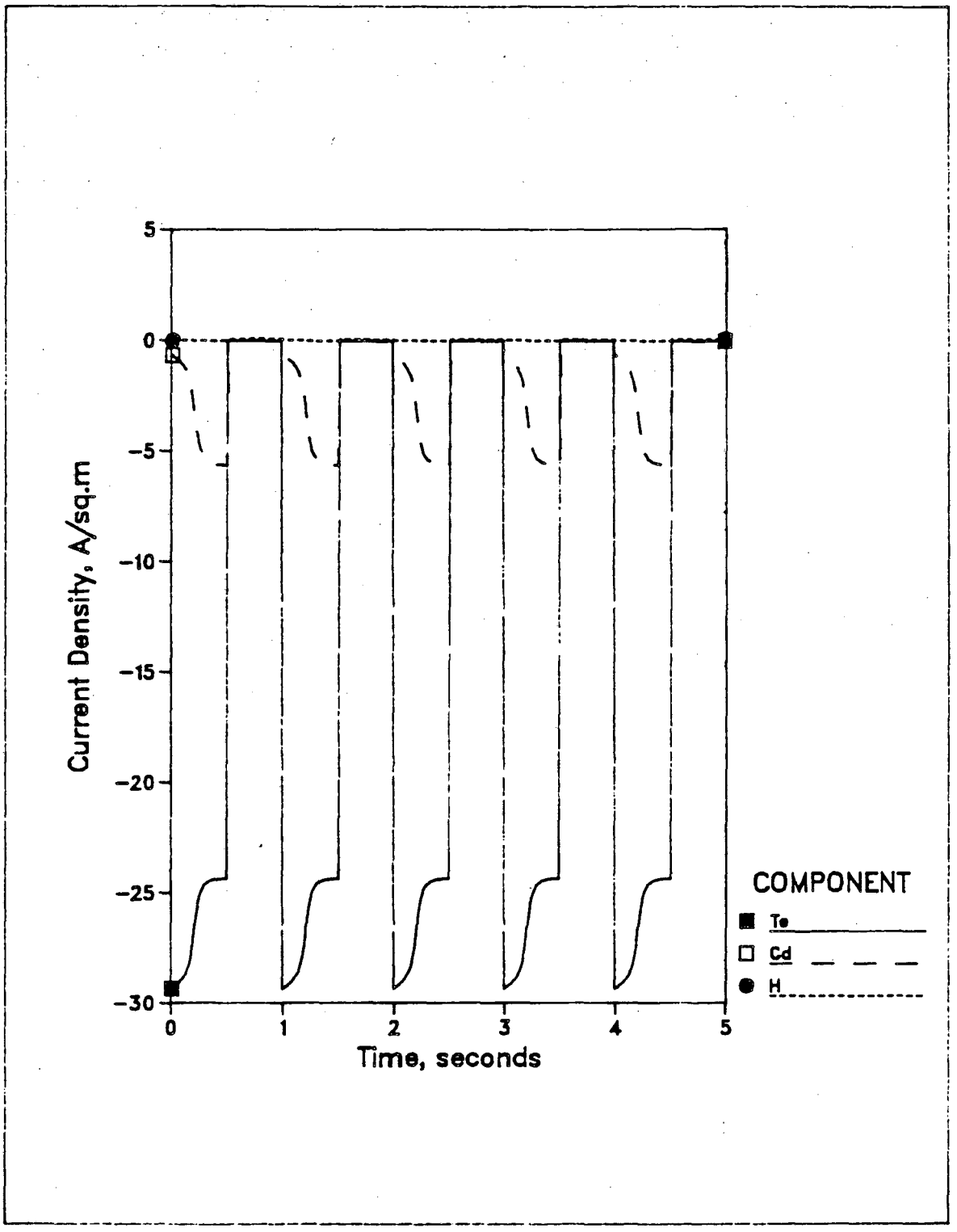
5
0
-5
-10
-15
-20
-25
-30
Current Density, A/sq.m
0
1
2
3
4
5
Time, seconds
COMPONENT
Te
Cd
H

FIGURE 10.

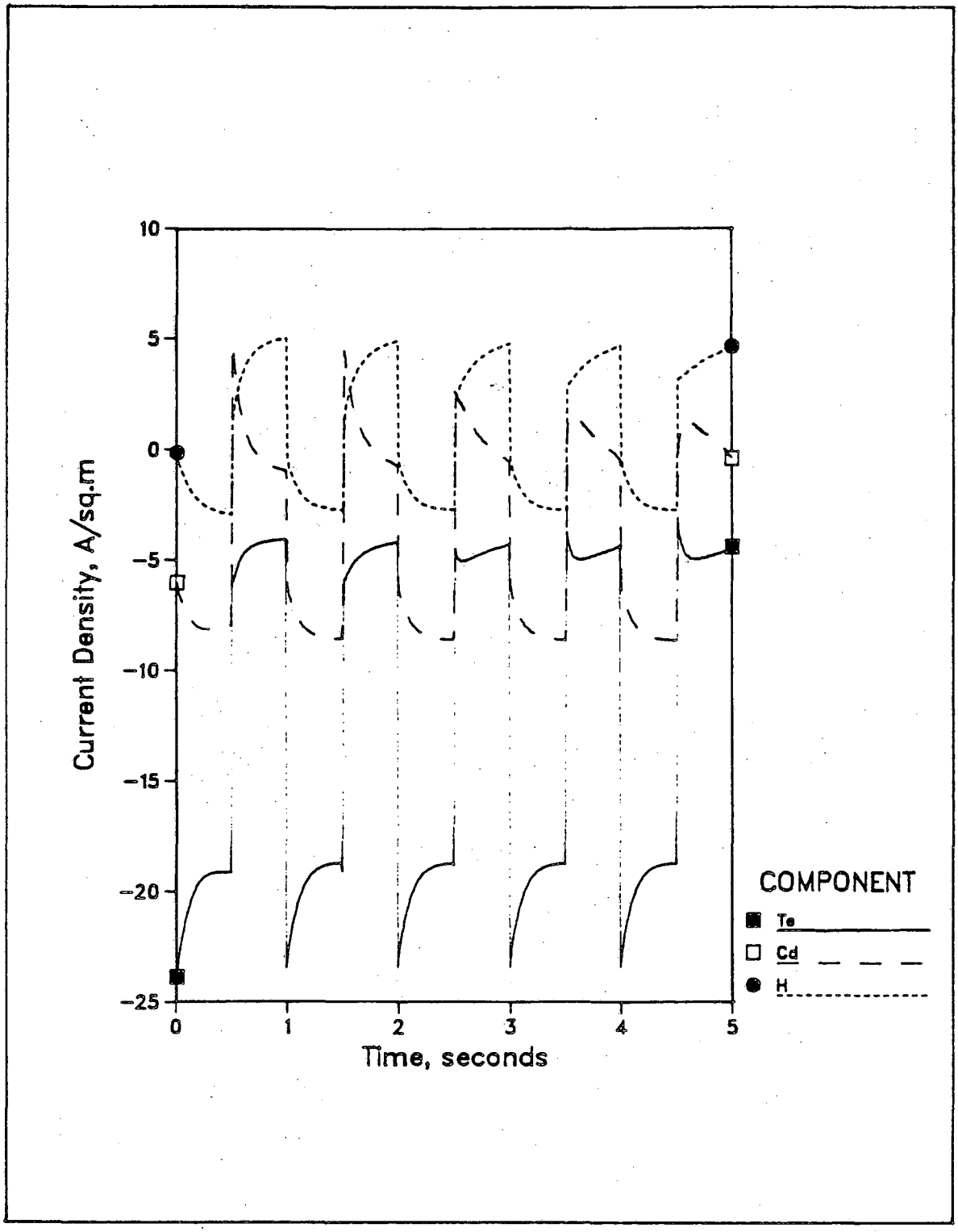
10
5
0
−5
−10
−15
−20
−25
Current Density, A/sq.m
0
1
2
3
4
5
Time, seconds
COMPONENT
Te
Cd
H

FIGURE 11.

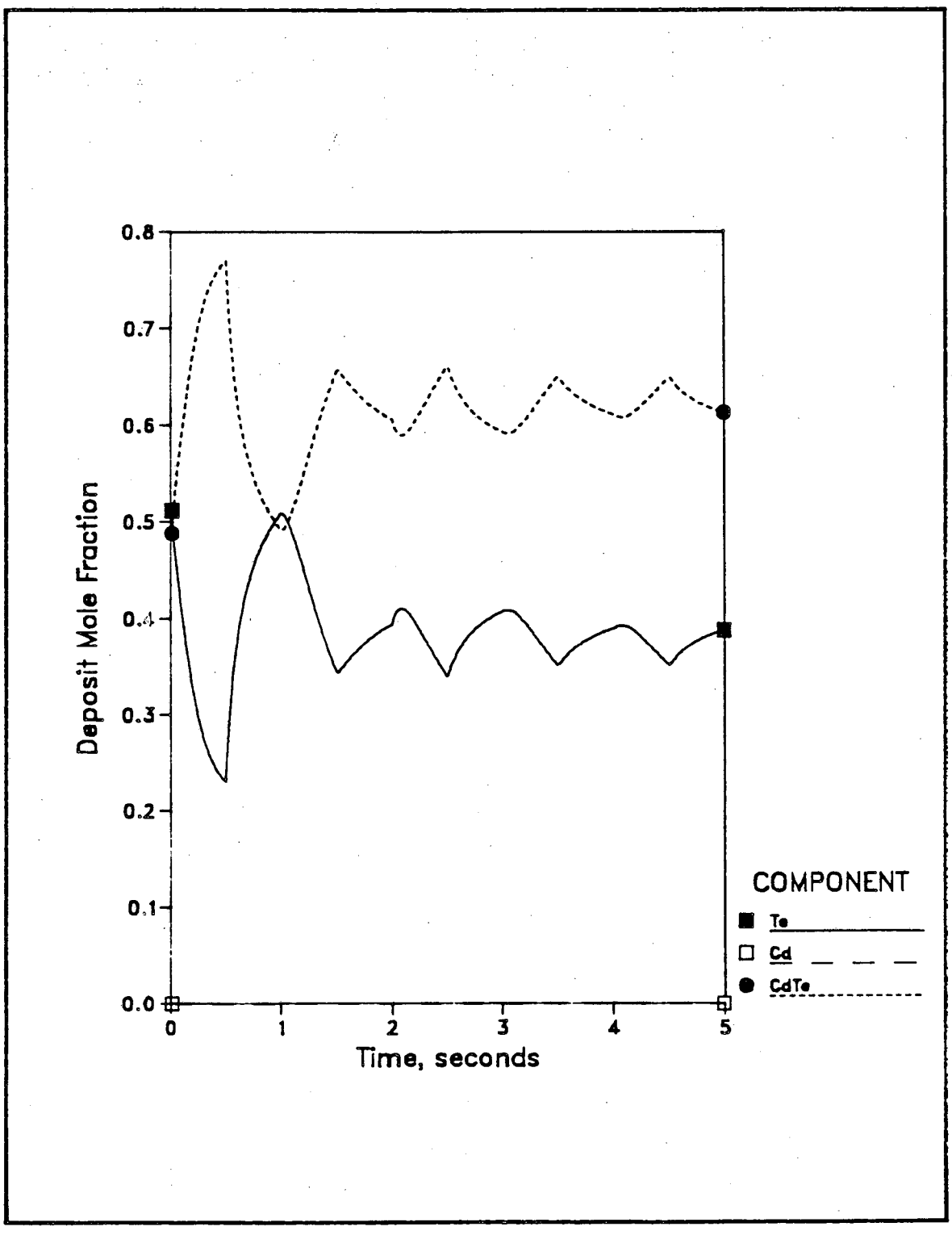
0.8
0.7
0.6
0.5
0.4
0.3
0.2
0.1
0.0
Deposit Mole Fraction
0
1
2
3
4
5
Time, seconds
COMPONENT
Te
Cd
CdTe

FIGURE 12.

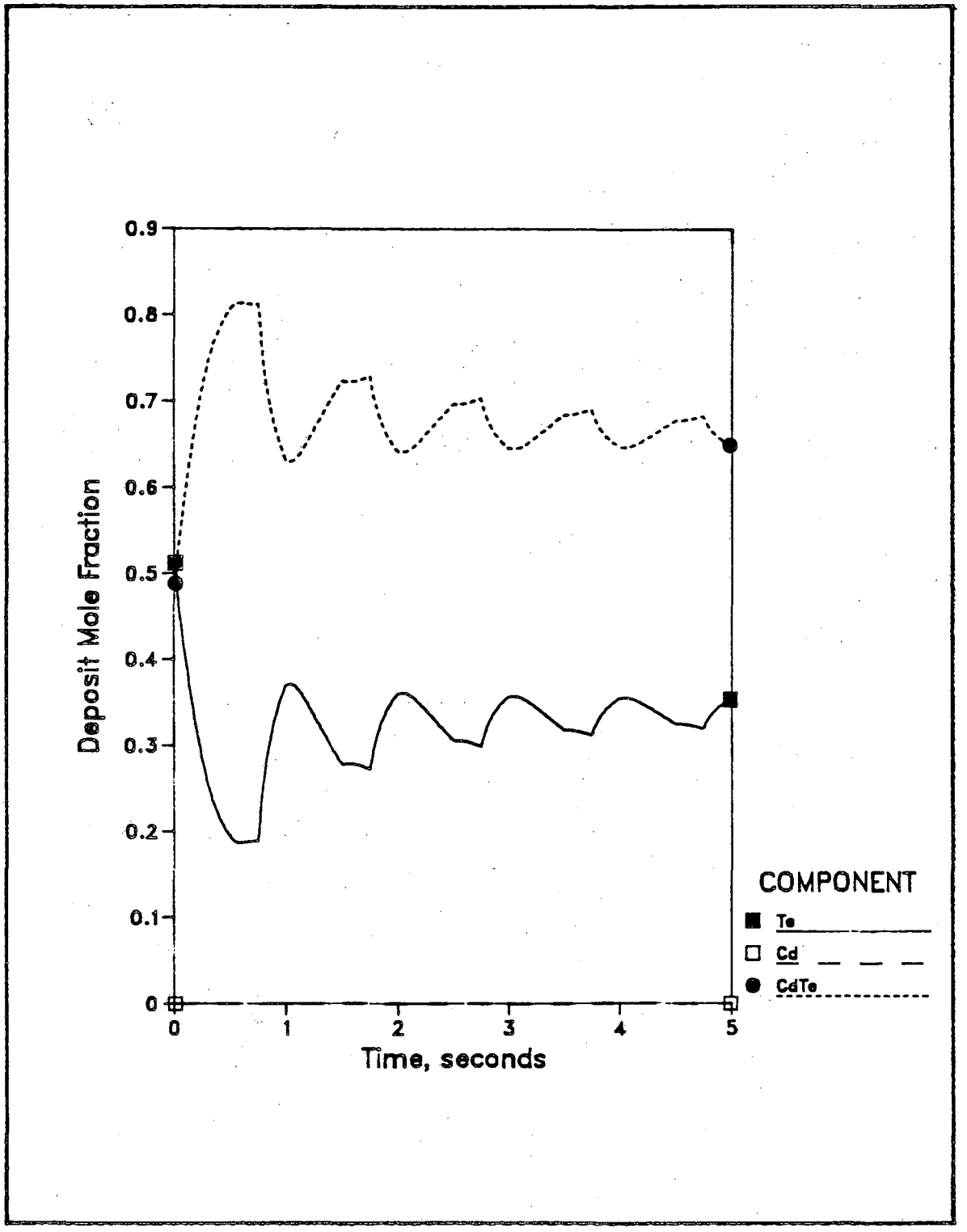
0.9
0.8
0.7
0.6
0.5
0.4
0.3
0.2
0.1
0
Deposit Mole Fraction
0
1
2
3
4
5
Time, seconds
COMPONENT
Te
Cd
CdTe

FIGURE 13.

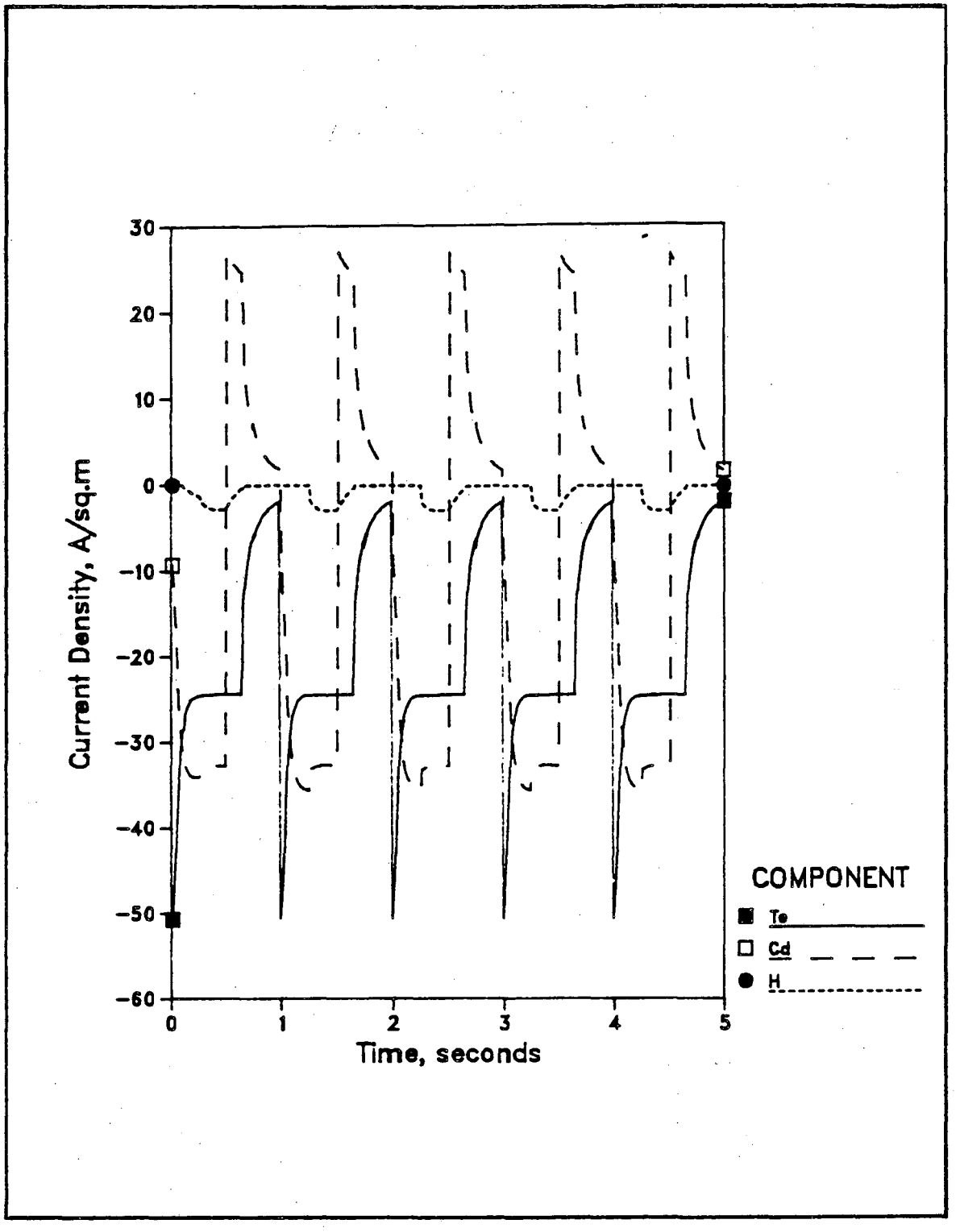
30
20
10
0
-10
-20
-30
-40
-50
-60
Current Density, A/sq.m
0
1
2
3
4
5
Time, seconds
COMPONENT
To
Cd
H

FIGURE 14.

This report was done with support from the Department of Energy. Any conclusions or opinions expressed in this report represent solely those of the author(s) and not necessarily those of The Regents of the University of California, the Lawrence Berkeley Laboratory or the Department of Energy.

Reference to a company or product name does not imply approval or recommendation of the product by the University of California or the U.S. Department of Energy to the exclusion of others that may be suitable.

LAWRENCE BERKELEY LABORATORY
TECHNICAL INFORMATION DEPARTMENT
UNIVERSITY OF CALIFORNIA
BERKELEY, CALIFORNIA 94720